J. Cent. South Univ. (2013) 20: 640–647
DOI: 10.1007/s11771-013-1530-y

Springer

Effect of static transmission error on dynamic responses of spiral bevel gears

TANG Jin-yuan(唐进元), HU Ze-hua(胡泽华), WU Li-juan(吴丽娟), CHEN Si-yu(陈思雨)

State Key Laboratory of High Performance Complex Manufacturing, (Central South University), Changsha 410083, China

Abstract: The effect of static transmission error on nonlinear dynamic response of the spiral bevel gear system combining with time-varying stiffness and backlash was investigated. Firstly, two different control equations of the spiral bevel gear model were adopted, where the static transmission error was expressed in two patterns as predesigned parabolic function and sine function of transmission errors. The dynamic response, bifurcation map, time domain response, phase curve and Poincare map were obtained by applying the explicit Runge-Kutta integration routine with variable-step. A comparative study was carried out and some profound phenomena were detected. The results show that there are many different kinds of tooth rattling phenomena at low speed. With the increase of speed, the system enters into stable motion without any rattling in the region (0.72, 1.64), which indicates that the system with predesigned parabolic function of transmission error has preferable capability at high speed.

Key words: spiral bevel gear; static transmission error; dynamic response; bifurcation

1 Introduction

Gear pair is the most extensive mechanism for transmission power and motion in various machineries and equipments. Spiral bevel gears and hypoid gears are the most complicated gear transmission systems, which are widely used in industrial departments such as the field of aeronautics, astronautics, transportation and instrument manufacturing [1–4]. As for the research of the dynamic response of spur gears and helical gears, KAHRAMAN and SINGH [5] presented and solved the dynamic equations with backlash and transmission error in the involute cylindrical gear model. Combined with the harmonic balance method, jump frequency, sub-harmonic resonance and chaotic phenomena were detected, though the model was of single degree of freedom (SDOF) with a constant stiffness.

Subsequently, lots of literature had been focusing on the research of nonlinear gear dynamics. However, due to the complexities of the gear surface and the gear mesh, there were few studies about spiral bevel gears. The current literature concentrated on the tooth contact analysis (TCA) at the static or quasi-static state [6–12]. GOSSELIN et al [11] proposed an LTCA method to analyze the dynamic error of spiral bevel gears with load, and the effects of the shape and amplitude of the unloaded transmission error curve on the loaded dynamic behaviours were demonstrated. The comprehensive deformation and contact deformation deduced by bend deformation and shear deformation were considered and improved, and the initial contact surface departure deduced by assembly error was analyzed as well. SIMON [12] studied the effect of motion deviation, adjustment error of the pinion shaft and angle error on the shape, location of contact zones and on the potential line of action. LITVIN et al [6–9] adopted the predesigned parabolic static transmission error to modify the spiral bevel gears, and excellent transmission properties were obtained with tooth contact analysis, which were all based on static analyses.

For the nonlinear dynamics of spiral bevel gears, YANG et al [13] established an SDOF hypoid gear dynamic equation, which included the time-varying stiffness, transmission error and backlash, and obtained the FFT responses by using the shooting method and continuous parameter method. WANG et al [14] established a 7-DOF nonlinear dynamic model of the spiral bevel gear with the dynamic relative transmission error, backlash and time-varying stiffness. The vibration displacement and velocity in the torsional, horizontal and vertical directions in the spiral bevel gear model under different conditions were depicted. The system entered into period doubling bifurcation and chaotic motion, and

Foundation item: Project(2011CB706800) supported by the National Basic Research Program of China; Project(51275530) supported by the National Natural Science Foundation of China
Received date: 2012–03–05; **Accepted date:** 2012–05–14
Corresponding author: CHEN Si-yu, PhD; Tel:+86–731–88877746; E-mail: csyd5053@yahoo.com.cn

the jump phenomena were detected with the varying mesh frequency. A 14-DOF system including time-varying mesh stiffness, transmission error and backlash was implemented by CHENG and LIM [15]. Transmission error was considered as the main excitation source and the dynamic responses were discussed. Sub-harmonic resonance and jump phenomena caused by the backlash of the tooth face under light load were detected. WANG et al [16] exhibited a hypoid gear vibration model with the consideration of nonlinear backlash, time-varying mesh points, time-varying mesh direction, time-varying mesh stiffness and dynamic transmission error, and the mesh parameters were denoted as harmonic components. The effect of time-varying mesh stiffness, static transmission error and load on the dynamic responses was included and demonstrated.

The main parameters discussed previously were time-varying mesh stiffness and nonlinear backlash, and the static transmission error and time-varying mesh stiffness were unfolded as Flouries series. For the static analyses and design, parabolic transmission error was the optimum transmission error curve. Combined with the model of spiral bevel gear transmission system [16], in this work, a comparative study was conducted, which focused on the different effects of parabolic transmission error and sine transmission error on the gear dynamics.

2 Gear model

The model of spiral bevel gears transmission system is shown in Fig. 1, and the parameters are listed in Table 1.

From Fig. 1, the torsional vibration equations of gear transmission system could be expressed as

$$I_{\mathrm{p}}\ddot{\theta}_{\mathrm{p}}+\tilde{\lambda}_{\mathrm{p}}\tilde{c}_{\mathrm{m}}\left(\tilde{\lambda}_{\mathrm{p}}\dot{\theta}_{\mathrm{p}}-\tilde{\lambda}_{\mathrm{g}}\dot{\theta}_{\mathrm{g}}-\dot{\tilde{e}}\right)+\tilde{\lambda}_{\mathrm{p}}\tilde{k}_{\mathrm{m}}f(\tilde{\lambda}_{\mathrm{p}}\theta_{\mathrm{p}}-\tilde{\lambda}_{\mathrm{g}}\theta_{\mathrm{g}}-\tilde{e})=T_{\mathrm{p}} \tag{1}$$

$$I_{\mathrm{g}}\ddot{\theta}_{\mathrm{g}}-\tilde{\lambda}_{\mathrm{g}}\tilde{c}_{\mathrm{m}}(\tilde{\lambda}_{\mathrm{p}}\dot{\theta}_{\mathrm{p}}-\tilde{\lambda}_{\mathrm{g}}\dot{\theta}_{\mathrm{g}}-\dot{\tilde{e}})-\tilde{\lambda}_{\mathrm{g}}\tilde{k}_{\mathrm{m}}f(\tilde{\lambda}_{\mathrm{p}}\theta_{\mathrm{p}}-\tilde{\lambda}_{\mathrm{g}}\theta_{\mathrm{g}}-\tilde{e})=-T_{\mathrm{g}} \tag{2}$$

where I_{p} and I_{g} are the moments of inertia of the pinion and gear, respectively; T_{p} and T_{g} are the torques of transmission gear pairs; $\tilde{c}_{\mathrm{m}}$ and $\tilde{k}_{\mathrm{m}}$ are the damping ratio and mesh stiffness of gear pairs, respectively. The backlash equation could be expressed as

$$f\left(\tilde{\lambda}_{\mathrm{p}}\theta_{\mathrm{p}}-\tilde{\lambda}_{\mathrm{g}}\theta_{\mathrm{g}}-\tilde{e}\right)=\begin{cases}\tilde{\lambda}_{\mathrm{p}}\theta_{\mathrm{p}}-\tilde{\lambda}_{\mathrm{g}}\theta_{\mathrm{g}}-\tilde{e}-b, & \tilde{\lambda}_{\mathrm{p}}\theta_{\mathrm{p}}-\tilde{\lambda}_{\mathrm{g}}\theta_{\mathrm{g}}-\tilde{e}>b\\ 0, & \left|\tilde{\lambda}_{\mathrm{p}}\theta_{\mathrm{p}}-\tilde{\lambda}_{\mathrm{g}}\theta_{\mathrm{g}}-\tilde{e}\right|\le b\\ \tilde{\lambda}_{\mathrm{p}}\theta_{\mathrm{p}}-\tilde{\lambda}_{\mathrm{g}}\theta_{\mathrm{g}}-\tilde{e}+b, & \tilde{\lambda}_{\mathrm{p}}\theta_{\mathrm{p}}-\tilde{\lambda}_{\mathrm{g}}\theta_{\mathrm{g}}-\tilde{e}<-b\end{cases} \tag{3}$$

where $2b$ is the backlash of gear pairs. $\tilde{\lambda}_{\mathrm{p}}$ and $\tilde{\lambda}_{\mathrm{g}}$ are the directional rotation radii of the pinion and gear, respectively, which could be denoted as

$$\tilde{\lambda}_{\mathrm{p}}=\boldsymbol{n}_{\mathrm{p}}\cdot\left(\boldsymbol{j}_{\mathrm{p}}\times\boldsymbol{r}_{\mathrm{p}}\right) \tag{4}$$

$$\tilde{\lambda}_{\mathrm{g}}=\boldsymbol{n}_{\mathrm{g}}\cdot\left(\boldsymbol{r}_{\mathrm{g}}\times\boldsymbol{j}_{\mathrm{g}}\right) \tag{5}$$

where $\boldsymbol{r}_{\mathrm{p}}$ and $\boldsymbol{r}_{\mathrm{g}}$ are the position vectors of mesh points of the pinion and gear, respectively; $\boldsymbol{n}_{\mathrm{p}}$ and $\boldsymbol{n}_{\mathrm{g}}$ are the unit normal vectors of mesh point; $\boldsymbol{j}_{\mathrm{p}}$ and $\boldsymbol{j}_{\mathrm{g}}$ are the unit vectors along pinion and gear rotating axes.

Because $\tilde{\lambda}_{\mathrm{p}}$ and $\tilde{\lambda}_{\mathrm{g}}$ are slowly changing parameters, then $\dot{\tilde{\lambda}}_l=\ddot{\tilde{\lambda}}_l=0$ and set $\tilde{x}=\tilde{\lambda}_{\mathrm{p}}\theta_{\mathrm{p}}-\tilde{\lambda}_{\mathrm{g}}\theta_{\mathrm{g}}-\tilde{e}$.

$$m_{\mathrm{e}}\ddot{\tilde{x}}+\tilde{c}_{\mathrm{m}}\dot{\tilde{x}}+\tilde{k}_{\mathrm{m}}f\left(\tilde{x}\right)=m_{\mathrm{e}}\left(\frac{\tilde{\lambda}_{\mathrm{p}}T_{\mathrm{p}}}{I_{\mathrm{p}}}+\frac{\tilde{\lambda}_{\mathrm{g}}T_{\mathrm{g}}}{I_{\mathrm{g}}}-\ddot{\tilde{e}}\right) \tag{6}$$

And the equivalent mass and backlash equations are

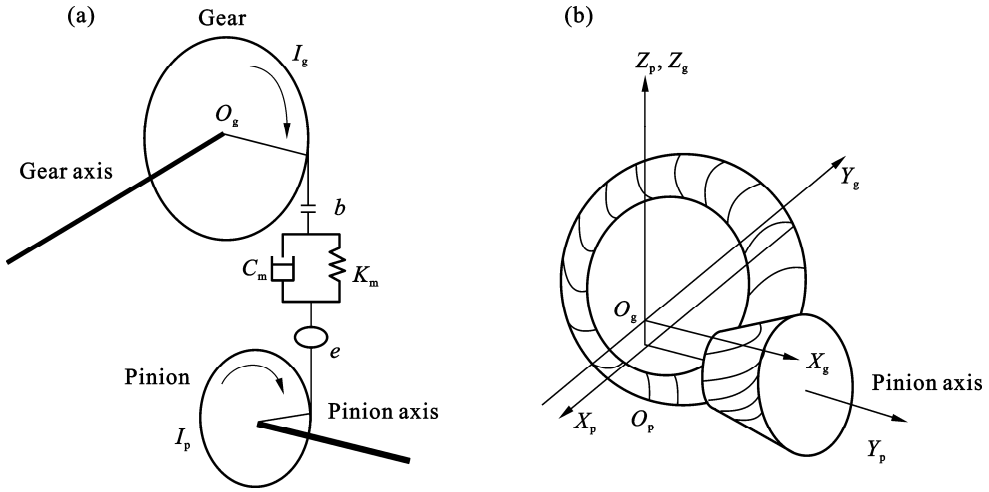

Fig. 1 Torsion model of spiral bevel gear: (a) Torsional vibration model of spiral bevel gear; (b) Coordinate systems for pinion and gear

Table 1 Gear parameters and their values

Gear parameter	Value
Pinion tooth number	10
Gear tooth number	43
Offset of pinion/m	0.031 8
Radius of pinion/m	0.048
Radius of gear/m	0.168
Moment of inertia of pinion/(kg·m^2)	0.002
Moment of inertia of gear/(kg·m^2)	0.05
Backlash/μm	20
Damping ratio	0.03

$$m_{\mathrm{e}}=\frac{1}{\lambda_{\mathrm{p}}^2/I_{\mathrm{p}}+\lambda_{\mathrm{g}}^2/I_{\mathrm{g}}},\ f(\tilde{x})=\begin{cases}\tilde{x}-b,\ \tilde{x}>b\\ 0,\ |\tilde{x}|\le b\\ \tilde{x}+b,\ \tilde{x}<-b\end{cases} \tag{7}$$

Set dimensionless parameters $x=\tilde{x}/b$, $t=\omega_{\mathrm{n}}\tilde{t}$, $\omega=\tilde{\omega}/\omega_{\mathrm{n}}$, $\lambda_{\mathrm{p}}=\tilde{\lambda}_{\mathrm{p}}/\lambda_{\mathrm{pm}}$, $\lambda_{\mathrm{g}}=\tilde{\lambda}_{\mathrm{g}}/\lambda_{\mathrm{gm}}$, $k=\tilde{k}_{\mathrm{m}}/k_{\mathrm{mm}}$ and $e=\tilde{e}/b$, and substitute them into Eqs. (6) and (7), then get

$$\ddot{x}+2\xi\left(\lambda_{\mathrm{p}}^2+\eta\lambda_{\mathrm{g}}^2\right)\dot{x}+\frac{\lambda_{\mathrm{p}}^2+\eta\lambda_{\mathrm{g}}^2}{1+\eta}kf(x)=f_{\mathrm{g}}\left(\lambda_{\mathrm{p}}+\lambda_{\mathrm{g}}\eta\right)-\ddot{e} \tag{8}$$

where

$$\begin{cases}\omega_{\mathrm{n}}=\sqrt{k_{\mathrm{mm}}/m_{\mathrm{em}}},\ m_{\mathrm{em}}=\dfrac{1}{\lambda_{\mathrm{pm}}^2/I_{\mathrm{p}}+\lambda_{\mathrm{gm}}^2/I_{\mathrm{g}}},\ \xi=\dfrac{\lambda_{\mathrm{pm}}^2\tilde{c}_{\mathrm{m}}}{\omega_{\mathrm{n}}},\\ \eta=\dfrac{\lambda_{\mathrm{gm}}^2 I_{\mathrm{p}}}{\lambda_{\mathrm{pm}}^2 I_{\mathrm{p}}},\ f_{\mathrm{g}}=\dfrac{\lambda_{\mathrm{pm}}T_{\mathrm{p}}}{b\omega_{\mathrm{n}}^2 I_{\mathrm{p}}},\ f(x)=\begin{cases}x-1,\ x>1\\ 0,\ |x|\le 1\\ x+1,\ x<-1\end{cases}\end{cases} \tag{9}$$

According to the characteristics of the gear mesh period, the varying parameters λ_{p}, λ_{g} and k with the variation of mesh points could be expressed as the Fourier series in the fundamental harmonic form:

$$\lambda_{\mathrm{p}}=1+\sum_{j=1}^{+\infty}\lambda_{\mathrm{p}aj}\cos\left(\mathrm{j}\omega t+\phi_{\mathrm{p}j}\right) \tag{10}$$

$$\lambda_{\mathrm{g}}=1+\sum_{j=1}^{+\infty}\lambda_{\mathrm{g}aj}\cos\left(\mathrm{j}\omega t+\phi_{\mathrm{g}j}\right) \tag{11}$$

$$k=1+\sum_{j=1}^{+\infty}k_{aj}\cos\left(\mathrm{j}\omega t+\phi_{kj}\right) \tag{12}$$

Gear transmission error was deduced from the gear machining errors, assembly errors and manufacturing errors, which made the gear mesh profile deviate from the theoretical mesh position and the correct mesh way of involute gear was destroyed. And the instantaneous transmission ratio varied and deduced collision and impact, which carried out the error excitation of gear mesh. The measured error value as the error excitation could describe the actual situation explicitly. For the restrictions of measurement conditions and time, it was hard to accomplish.

In the present literature on the nonlinear dynamics of spiral bevel gears [13–16], according to the accumulation tolerances of the standard tooth space based on the accuracy grade of spiral bevel gears and hypoid gears, the static transmission error was simulated as harmonic function:

$$e=e_0+\sum_{j=1}^{+\infty}e_{rj}\cos\left(\mathrm{j}\omega t+\phi_{rj}\right) \tag{13}$$

Transmission error was regarded as the main excitation of the gear noise and vibration of the gear. The static transmission error was predesigned as parabolic format in design process, which could incorporate the linear error deduced from the misalignment of the gear shaft. The method was marvelously applied in the quasi-static analyses, and could reduce vibration and noise obviously. The pre-design parabolic transmission error in the mesh surface of the gear pairs could be expressed as

$$\psi(t)=-at^2 \tag{14}$$

The whole motion graph, as shown in Fig. 2, could be plotted when the transmission error curves on one pair gear tooth surface were plotted as the period of $T_{\mathrm{n}}=2\pi/N_{\mathrm{p}}$ repeatedly.

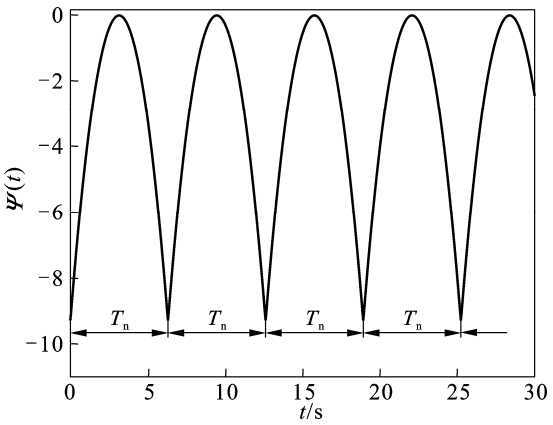

Fig. 2 Parabolic static transmission error

Equation (8) shows that the static transmission error (STE) in the nonlinear model came out at the second derivative, and the second derivative of the parabolic transmission error is shown in Fig. 3. It is an impulse excitation, which is quite different from the traditional

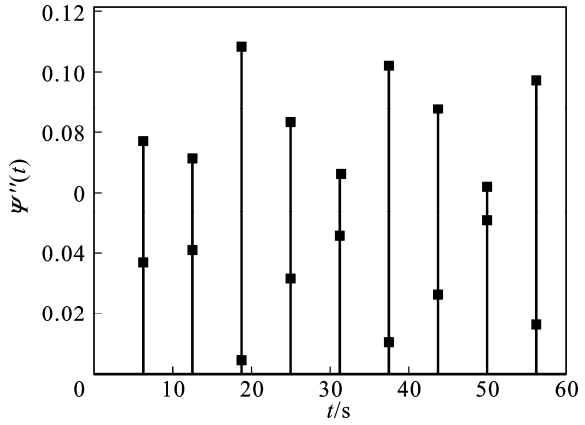

Fig. 3 Second derivative of parabolic transmission error

dynamic model of gear transmission system. To avoid the situation referred above, an assumption should be made as

$$x_1 = \tilde{\lambda}_p \theta_p - \tilde{\lambda}_g \theta_g \tag{15}$$

Then,

$$\tilde{x} = x_1 - \tilde{e} \tag{16}$$

Substituting Eq. (16) into Eq. (8), it could be simplified as

$$\ddot{x}_1 + 2\xi\left(\lambda_p^2 + \eta\lambda_g^2\right)\dot{x}_1 + \frac{\lambda_p^2 + \eta\lambda_g^2}{1+\eta} kf\left(x_1 - e\right) = f_g\left(\lambda_p + \lambda_g\eta\right) + 2\xi\left(\lambda_p^2 + \eta\lambda_g^2\right)\dot{e} \tag{17}$$

where

$$f\left(x_1 - e\right) = \begin{cases} x_1 - \left(e+1\right), & x_1 - e > 1 \\ 0, & \left|x_1 - e\right| \le 1 \\ x_1 - \left(e-1\right), & x_1 - e < -1 \end{cases} \tag{18}$$

To study the STE of spiral bevel gears, two different equations of analytical models, Eq. (8) and Eq. (17) were established, both of which could represent the dynamic characteristics of the gear system. STE was an analytical method based on the static or quasi-static states. However, it was not certain to suppress the vibration and noise in actual motion process. And, the value of parameter a should to be set suitably. To tackle the problems, a comparative study was conducted under the two models, focusing on the effect of STE on the characteristics of dynamic responses of spiral bevel gears.

3 Comparison of two models

The diversity of gear dynamic responses in two different models was discussed. And the high-order harmonic components of parameters such as λ_p, λ_g, k and e varying with mesh points were ignored. Set the systematic parameters as f_p=2, ξ_p=0.03, e_{r1}=0.5, k_{a1}=0.5, λ_{pa}=λ_{ga}=0.01, η=0.75, ϕ_{p1}=ϕ_{g1}=0, ϕ_{k1}=–4π/5, ϕ_{r1}=0. The system response curves of Eq. (8) and Eq. (17) are plotted in Figs. 4(a) and 4(b), respectively, where the horizontal vector stands for the pinion rotational frequency ω, and the vertical vector stands for the root-mean-square (RMS) value of the steady state responses x_{rms} [17].

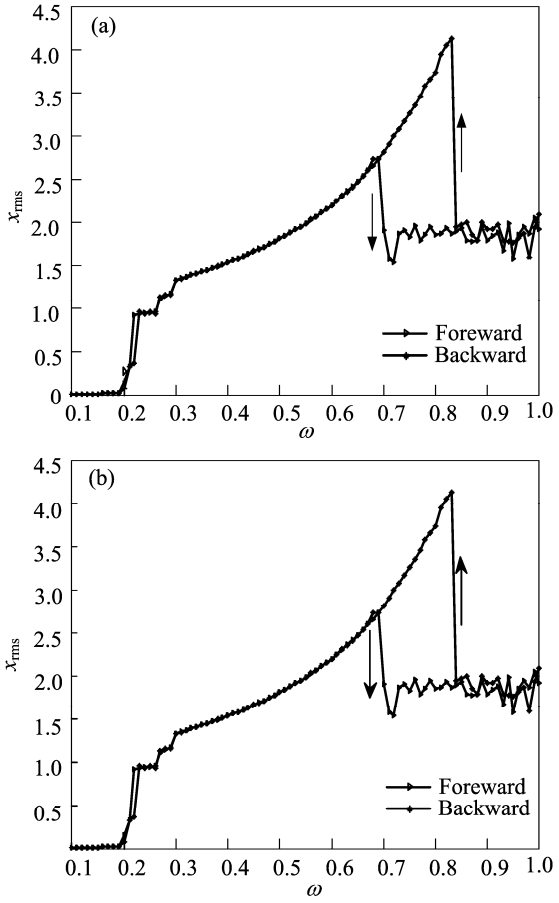

Fig. 4 Response curves of two different models; (a) Sine STE case; (b) Pre-design parabolic STE case

For Eq. (8), with the increase of frequency ω in the zone [0.01, 1] (as positive sweep frequency), the response curve of the gear system is plotted in Fig. 4(a) and the arrow denotes the jump direction. The amplitude value jumps at x_{rms}=1.235 and ω=0.27 and then enters into steady state motion, so the system is under single-sided impact. However, the second jump phenomenon appears at ω=0.71 and the system enters into chaotic motion. When the value of ω decreases from 1 to 0.01 (in negative sweep frequency), the response curve of the gear system is plotted. The system stays in chaotic state at high frequency. With the decrease of frequency ω, the jump phenomenon is detected at ω=0.83, and then enters into steady state motion. From the description of Fig. 4, we can conclude that

co-existing solutions exist in the zone (0.725, 0.835), which is corresponding to the calculation and experiment results in Ref. [18]. We can see that a peak value appears at resonance frequency ω=0.3 in the system response from Eq. (17), as shown in Fig. 4(b). Moreover, the multi solution zone, which is in the zone (0.725, 0.815), is narrow compared to the situation of Eq. (8). All the above analyses can demonstrate that co-existing solutions and multi impact are carried out and equivalent in the two different models.

4 Effect of static transmission error

4.1 Effect of sine static transmission error

In this subsection, the effect of sine static transmission error on dynamic characteristics of the spiral bevel gear system is studied. Setting f_p=1, 3, the system parameters are the same as the previous subsection, and the response curves of the system are shown in Fig. 5. When the load is f_p=1, the results of the positive sweep frequency calculation are plotted in Fig. 5(a). The first upward jump phenomenon is detected at the mesh frequency ω=0.2 along with the increase of x_{rms}. With the increase of frequency ω, the system enters into chaotic motion and the downward jump appears around ω=0.7. The results of the negative sweep frequency are also plotted in Fig. 5(a). The value of x_{rms} is decreases and the system responses jump upward around ω=0.84 and then enter into steady motion. When the load is f_p=3, the results of the positive sweep frequency calculation are plotted in Fig. 5(b), and the value of x_{rms} oscillates around 2 at a low frequency period. The first upward jump is carried out at the mesh frequency ω=0.38 and x_{rms} reaches the peak value 3.15. The value of x_{rms} decreases with the increase of frequency ω. The system appears downward jump at ω=0.8 and enters into chaotic motion. The results of the negative sweep frequency are also plotted in Fig. 5(b), and both the values of frequency increase where upward jump and downward jump appear, and the two sweep frequency curves are crossed. All the analyses above can demonstrate that the value of load can affect the characteristics of the response extensively. With the increase of load, the jump frequency increases as well and the co-existing solution zones are altered obviously.

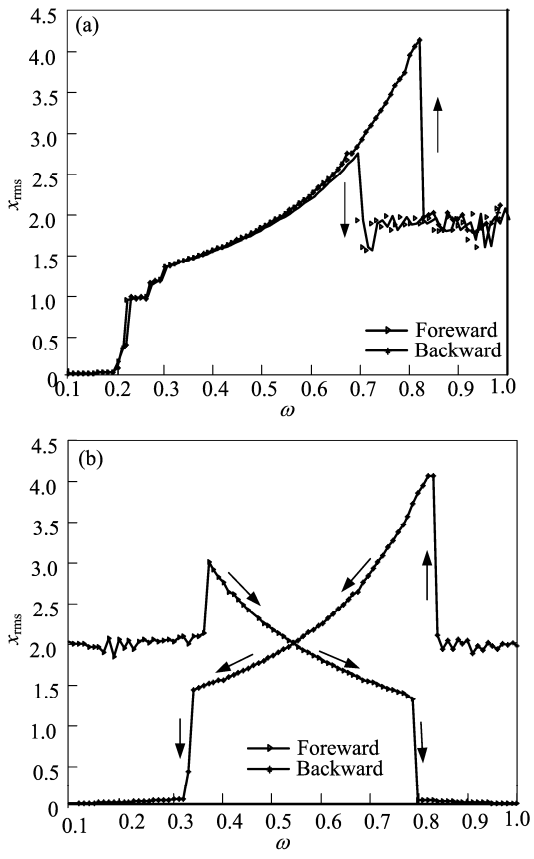

Fig. 5 System response curves with variation of loads: (a) f_p=1; (b) f_p=3

4.2 Effect of parabolic static transmission error

The system parameters are the same as referred previously. When the STE of the spiral bevel gear system is in pre-design parabolic form, the system response is shown in Fig. 6. At low velocity, the value of x_{rms} response is large and a little jump process exhibits. The positive and negative sweep frequency zones are (0.58, 0.70) and (0.56, 0.72), respectively. At high velocity, a downward jump appears at ω=1.64 in positive direction. Conversely, an upward jump appears at ω=1.74 in negative direction. With the comparative analyses, the nonlinear characteristics of the spiral bevel gear system are not transformed with the pre-design parabolic STE, and impact and frequency jump still exist in the system.

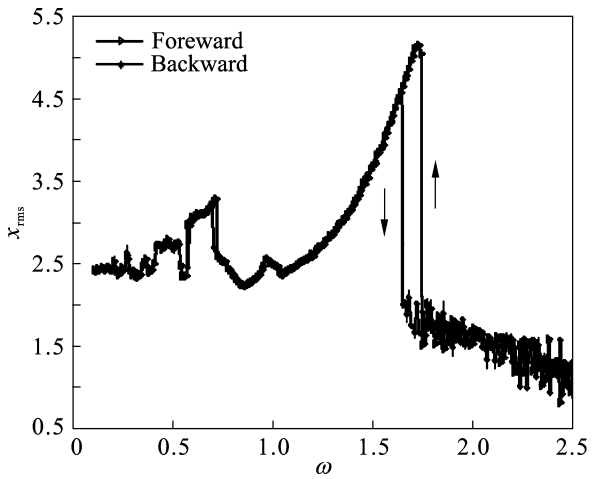

Fig. 6 System response with parabolic STE

The motion of the system is extremely unstable at low velocity in this case, and the vibration and impact are severe. On the contrary, the motion of the system is stable at high velocity, gear tooth impact and gear surface impact disappear, the jump frequency entering into chaotic motion increases and excellent high velocity property can be carried out.

4.3 Chaotic and bifurcation

When the load f_p=1, the displacement varying with mesh frequency ω in the Eq. (15) can be deduced, as shown in Fig. 7. The displacement varies obviously at low frequency zones, no obvious period doubling bifurcation appears and the system enters into chaotic motion at ω=0.48. With the increase of frequency, the

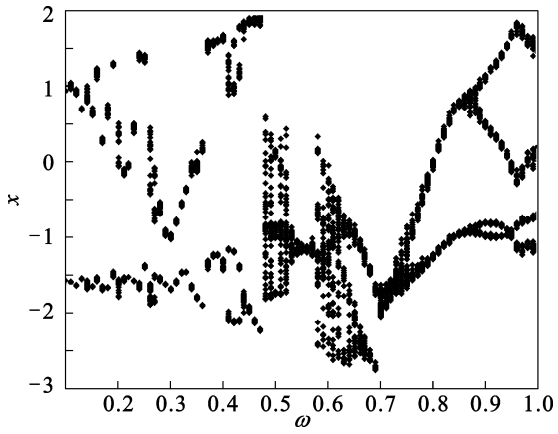

Fig. 7 Bifurcation graph at load f_p=1

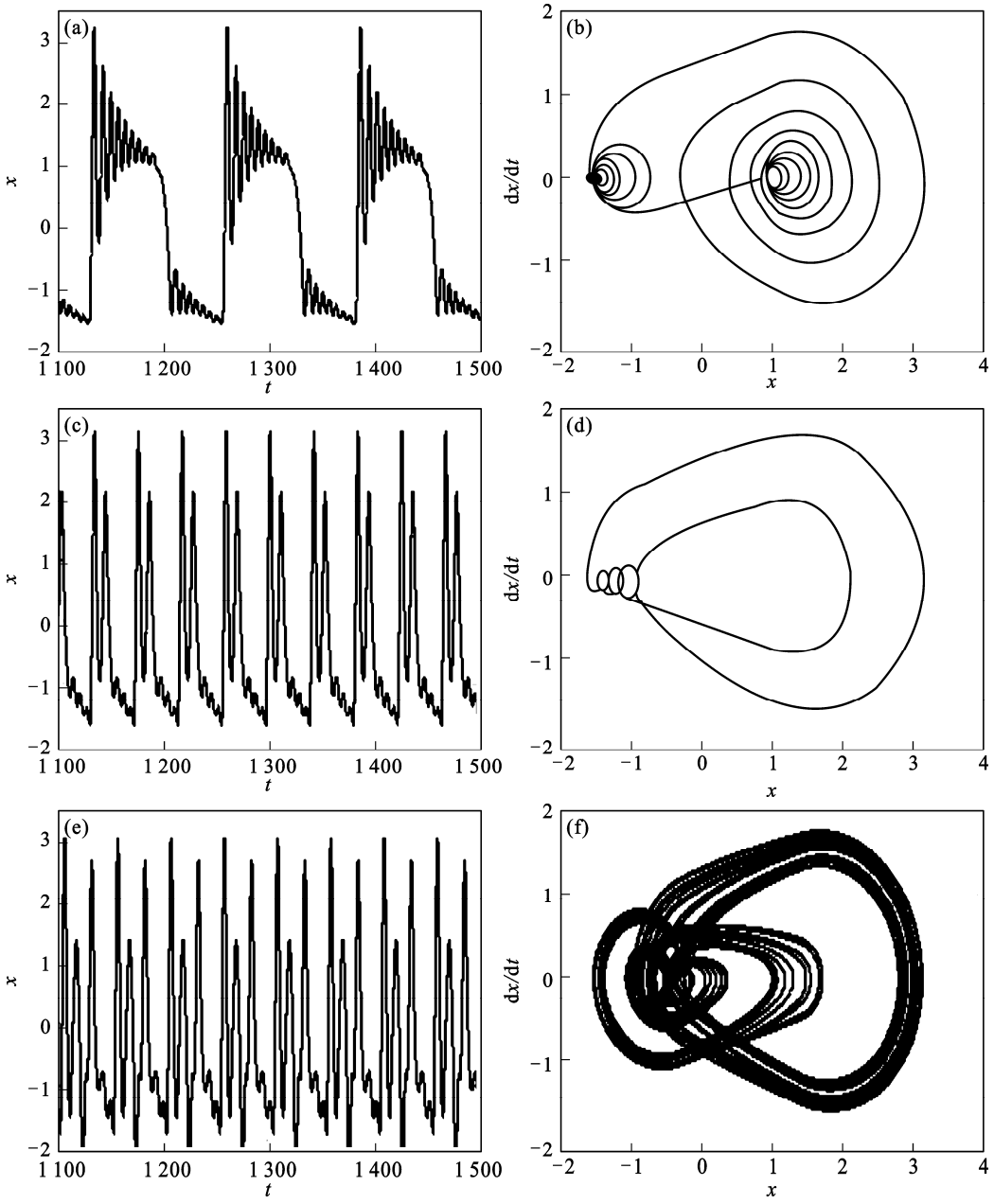

Fig. 8 Time domain response and phase space: (a), (b) ω=0.1; (c), (d) ω=0.3; (e), (f) ω=0.6

chaos is suppressed, and 2-period bifurcate enters into 4-period bifurcate obviously in the high frequency zone (0.8, 1). For the further study on the motion of the spiral bevel gear system, Fig. 8 exhibits the time domain responses and phase space graphs at ω=0.1, 0.3 and 0.6. The time domain response and phase space graph at ω=0.1 are plotted in Figs. 8(a) and (b), respectively. The displacement varies periodically, and the period is $2T_n$. In the first period T_n, the oscillation amplitude is large, the gear tooth impact is serious, and the vibration impact decreases until the tooth pair mesh departure. In the second period T_n, the mesh departure changes into tooth back impact, and gear tooth surface impact, mesh departure and tooth back impact appear periodically. The time domain response and phase space graph at ω=0.3 are plotted in Figs. 8(c) and (d), respectively. The period of displacement is $T_n/2$, and the tooth surface impact and tooth back impact decrease a little. The time domain response and phase space graph at ω=0.6 are plotted in Figs. 8(e) and (f), respectively. The system is in chaotic motion, and the tooth surface impact and tooth back impact still exist. Moreover, the motion is disordered. The Poincare mappings of the system responses at ω=0.5 and ω=0.6 are plotted in Fig. 9. And we can infer that the Poincare mapping is narrow in two tortuous curves zone at ω=0.5. With the increase of frequency ω, the phase space is twisted and rotated in a certain angle, as shown in Fig. 9(b).

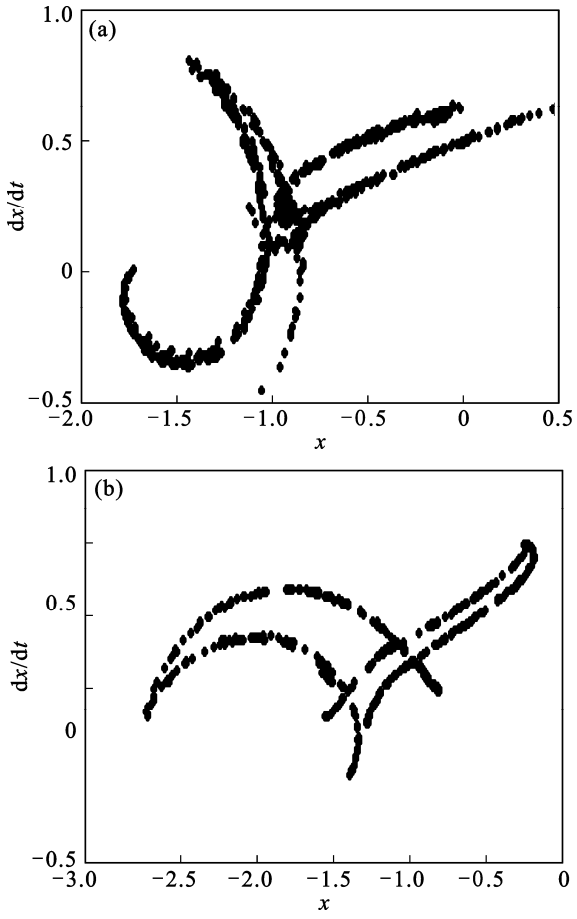

Fig. 9 Poincare mapping: (a) ω=0.5; (b) ω=0.6

5 Conclusions

1) The nonlinear characteristics of the two dynamic equations in the spiral bevel gear transmission system are equivalent such as frequency jump and chaos. Only the values of jump frequency and those of the chaotic frequency have slight differences.

2) When the excitation is in sine format, the performance of the spiral bevel gear transmission system at low velocity is high and weak gear tooth surface impact exists. However, the frequency value of jumping into chaos is no larger than 0.9, which implies that the performance of the system at high velocity under the excitation situation is poor.

3) When the excitation is in parabolic format, the property of the spiral bevel gear transmission system at low velocity is limited with the severe gear tooth surface impact, tooth back impact and tooth mesh departure. The gear transmission motion tends to be steady with the increase of velocity. No gear tooth impact exists in the frequency zone (0.72, 1.64), and upward jump phenomenon is observed at ω=1.74 in the negative sweep frequency direction, which can demonstrate that the property of the system at high velocity under this excitation is excellent.

4) Various forms of gear tooth surface impact and tooth back impact in the spiral bevel gear transmission system are detected. The mesh process of the spiral bevel gears at low velocity is a continuous action of mesh and impact.

References

[1] LI Ming, SUN Tao, HU Hai-yan. Review on dynamics of geared rotor-bearing systems [J]. Journal of Vibration Engineering, 2002, 15(3): 249–261. (in Chinese)

[2] LI Run-fang, WANG Jian-jun. Gear system dynamics-vibration impact noise [M]. Beijing: Science Press, 1997: 2–9. (in Chinese)

[3] YANG Hong-bin, DENG Xiao-zhong, GAO Jian-ping, FANG Zong-de. Overview of the research on the non-linear oscillation of gears and a proposal for anti-vibration of spiral bevel and hypoid gears [J]. China Mechanical Engineering, 1999, 10(7): 807–809. (in Chinese)

[4] LIN Teng-jiao, LI Run-fang, GUO Xiao-dong, WANG Li-hua. Analyses of impact characteristics of three-dimensional nonlinear backlash of the hypoid gears [J]. China Mechanical Engineering, 2003, 14(9): 727–730. (in Chinese)

[5] KAHRAMAN A, SINGH R. Interactions between time varying mesh stiffness and clearance nonlinearities in a geared system [J]. Journal of Sound and Vibration, 1991, 146(1): 135–156.

[6] LITVIN F L. Gear Geometry and Applied theory [M]. Englewood Cliffs, NJ: Prentice Hall, 1994: 258–282.

[7] LITVIN F L, CHEN N X, CHEN J S. Computerized determination of curvature relations and contact ellipse for conjugate surfaces [J]. Computer Methods in Applied Mechanics and Engineering, 1995, 125(1): 151–170.

[8] LITVIN F L, ZHANG Y. Local synthesis and tooth contact analysis of face-milled spiral bevel gears NASA CR4342 [R]. Chicago: NASA Lewis Research Center, 1991.

[9] LITVIN F L, VECCHIATO D, GUROVICH E, FUENTES A, GONZALEZ-PEREA L, HAYASAKA K, YUKISHIMA K. Computerized development in design, generation, simulation of meshing, and stress analysis of gear drives [J]. Meccanica, 2005, 40(3): 291–324.

[10] ZHANG Jin-liang, FANG Zong-de, CAO Xue-mei, DENG Xiao-zhong. The modified pitch cone design of the hypoid gear manufacture, stress analysis and experimental tests [J]. Mechanism and Machine Theory, 2007, 42(2): 147–158.

[11] GOSSELIN C, CLOUTIER L, NGUYEN Q D. A general formulation for the calculation of the load sharing and transmission error under load of spiral bevel and hypoid gears [J]. Mechanism and Machine Theory, 1995, 30(3): 433–450.

[12] SIMON V. The influence of misalignments on mesh performances of hypoid gears [J]. Mechanism and Machine Theory, 1998, 33(8): 1277–1291.

[13] YANG Hong-bin, GAO Jian-ping, FANG Zong-de, DENG Xiao-zhong, ZHOU Yan-wei. Nonlinear dynamics of hypoid gears [J]. Automotive Engineering, 2002, 22(1): 51–54. (in Chinese)

[14] WANG San-ming, SHEN Yun-wen, DONG Hai-jun. Non-linear dynamical characteristics of a spiral bevel gear system with backlash and time-varying stiffness [J]. Chinese Journal of Mechanical Engineering, 2003, 39(2): 28–32. (in Chinese)

[15] CHENG Y, LIM T C. Dynamics of hypoid gear transmission with nonlinear time-varying mesh characteristics [J]. Trans ASME Journal of Mechanical Design, 2003, 125(6): 373–382.

[16] WANG Jun, LIM T C, LI Ming-feng. Dynamics of a hypoid gear pair considering the effects of time-varying mesh parameters and backlash nonlinearity [J]. Journal of Sound and Vibration, 2007, 308(1/2): 302–329.

[17] BLANKENSHIP G W, KAHRAMAN A. Steady state forced response of a mechanical oscillator with combined parametric excitation and clearance type non-linerity [J]. Journal of Sound and Vibration, 1995, 185(5): 743–765.

[18] KAHRAMAN A, SINGH R. Nonlinear dynamics of a spur gear pair [J]. Journal of Sound and Vibration, 1990, 142(1): 49–75.

(Edited by DENG Lü-xiang)